DC Electrical Resistance Tomography Inversion

Fallah Safari, M.[1] and Ghanati, R.[2*]

1. Ph.D. Graduated, Department of Earth Physics, Institute of Geophysics, University of Tehran, Tehran, Iran
2. Assistant Professor, Department of Earth Physics, Institute of Geophysics, University of Tehran, Tehran, Iran

Abstract

Direct current electrical resistivity imaging is provided by measuring the vertical and horizontal electrical potential variations of subsurface structures using surface and borehole records. To recover the resistivity tomograms from the observed data, a non-linear inverse problem is required to be iteratively solved. A 2.5-dimensional forward modeling based on the finite-difference method with rectangular meshes is also formulated. The two-dimensional reconstruction of earth resistivity data is implemented using a smoothness constrained inversion algorithm (i.e. Occam's method), wherein a Gauss-Newton technique for updating the sensitivity function is proposed. After verifying the accuracy and efficiency of the forward modeling and the sensitivity function calculation, the inversion algorithm is tested on synthetic data from both geometrically simple and complicated bodies and a real data set. A stopping criterion based on the noise level, roughly estimated using the method of reciprocal resistance measurements, is also provided leading to preventing over-or under-interpreted structure during the inversion process. The numerical experiments reveal that the proposed inversion algorithm provides stable inversion results and an acceptable representation of the main features and structure of the models without producing spurious effects. Furthermore, to deal with the reliability of the recovered models, a model sensitivity analysis is implemented using the resolution density distribution. All used formulations and concepts are part of a Matlab source code developed during this study.

Keywords: Electrical resistivity tomography, 2.5-D non-linear inversion, Resolution density.

1. Introduction

Geo-electrical approaches are intrinsically sensitive to discontinuities within the electrical characteristics of subsurface structures. Electrical resistivity tomography (ERT) is a well-established and widely used method to solve a variety of subsurface detection problems, e.g., engineering studies, environmental and hydro-geophysical investigations, and archaeological exploration. The ERT measurements are also applied to map geologic features such as lithology, structure, fractures, and stratigraphy; hydrologic features such as depth to the water table, depth to aquitard (impermeable layer), and groundwater salinity; and to delineate groundwater contaminants. As in any geophysical procedures, surface or borehole resistivity measurements do not provide a direct image of the Earth's subsurface but simply the integrated effect of the subsurface properties, which could be far removed from the ground truth, in particular, in cases of complex subsurface property distribution. To infer an image of the subsurface resistivity distribution from a limited number of uncertain observations, a non-linear inverse problem needs to be formulated. The inverse direct current resistivity problem is generally ill-posed with respect to data uncertainties and incomplete data sets. Hence, regularization schemes must be incorporated in the inverse problem to find a unique and stable solution. Even though regularization plays a significant role in inverse problem theory, there is a large ambiguity in choosing it (Scales and Snieder, 1997). The most commonly used techniques for regularization of inverse problems are: 1) the projection methods, such as truncated singular value decomposition, and 2) penalty methods, such as Tikhonov-Phillips regularization, and total variation methods. In the Tikhonov-Phillips method, the regularization term consists of the squared norm of the sought solutions. The quadratic regularization methods smear out the edges of the desired model but non-quadratic regularizations address the issue of stability without penalizing the required sharp boundaries. They usually require the solution to be sparse in a specific domain. Although non-quadratic regularization methods lead to further complexity of the problem compared to the quadratic approaches. For both of these approaches, a suitable regularization parameter should yield

---

*Corresponding author: rghanati@ut.ac.ir

a fair balance between the perturbation error and regularized solution. Whereas in most cases, the true subsurface geology exhibits a gradual variation in the electrical properties of layer boundaries, using the smoothness-constrained method is more suitable to visualize the Earth's structures. However, smoothing constraints are inconsistent with realistic circumstances when sharp bulk conductivity contrast exists in the subsurface. The development of direct resistivity inversions has progressed successfully. The first attempt for inversion of 2D resistivity data made by Pelton et al. (1978). Although their algorithm is not well suited to complex cases. Smith and Vozoff (1984) and Tripp et al. (1984) presented a 2D resistivity inversion using a finite-difference method. The schemes proposed by them are suitable for complicated 2D models but do not incorporate the effects of topography on resistivity data in the inversion algorithm. Tong and Yang (1990) developed an algorithm for 2D resistivity inversion where the topography is considered in the model. The paper of Loke and Barker (1996) proposed a Gauss-Newton-based algorithm for ERT inversion in the framework of finite-difference. In recent years, the introduction of multi-channel instrument resulted in a renaissance of the geo-electrical data acquisition, and consequently, significant progress in 2D and 3D inverse modeling algorithms (e.g., Dahlin and Zhou, 2001; Zhou and Dahlin, 2003; Günther et al., 2006; Chambers et al, 2006; Oldenborger et al., 2007; Wilkinson et al, 2008; Zhou et al., 2014; Pang et al., 2020). In addition, an integral part of every electrical resistivity inversion is an accurate and efficient forward modeling resulting in the numerical simulation of responses for a given conductivity model. A numerical technique for the 2.5 dimensional DC resistivity forward calculation based on the finite-difference method is provided. In this study, we developed and applied a model-space Occam's method to the electrical resistivity tomography inversion. Mathematically, Occam's inversion is a generalized least-squares inversion method under some specified model property constraint (Constable et al., 1987; De Groot-Hedlin and Constable, 1990). Thus it make the inversion

method more stable and robust. This algorithm converges even in complex subsurface property distribution where other inversion algorithms may fail. The efficiency and applicability of our numerical strategy for 2D resistivity inverse modeling is tested using two synthetic case studies as well as a real dataset. Furthermore, the reliability of the recovered models is dealt with through a model sensitivity analysis based on the resolution density distribution. The rest of the paper is structured as follows: Section 2 gives a brief review of the forward and inverse modeling formulation. Next, section 3 verifies the functionality of the inversion algorithm using synthetic and real resistivity data sets. Finally, section 4 provides a short conclusion and summary.

2. Methodology
In this section, a brief description of the forward calculation in the framework of the finite- difference method is first provided. Then, we extend the inversion algorithm based on the model-space Occam's method with the aim of seeking the smoothest or minimum structure model subject to a constraint on the misfit. In this study, the forward and inverse modeling codes are only developed with MATLAB scripts.

2-1. Forward modeling formulation
A first and significant step is to formulate and solve a 2.5-D direct current resistivity forward modeling routine. The advantage of the 2.5-D approach is that a physically realistic representation, involving full 3-D electrical potential distribution, is obtained by solving several problems with restricted 2-D geometry in the wave number domain. In this way, the computational time is reduced compared to a full 3D modeling. An accurate and efficient forward calculation is the basis of most processes of the inversion. Calculation of resistivity forward responses is carried out using simulation of the current flow into the earth's surface through solving Poisson's equation. In this contribution, a finite-difference algorithm is applied to discretize the simulated models restricted by a mixed boundary condition. One of the merits of the finite-difference method over the other methods is its well-known ability to quickly approximate the solutions for any

arbitrary and complex structure models. The finite-difference method is relatively fast compared with the finite-element method. However, to include a general topography, the finite-element method becomes a better selection despite being computationally expensive. The partial differential equations governing the resistivity problem are obtained by using the principle of conservation of charge and the continuity equation, we have for a point source $r_s(x_s. y_s. z_s)$ (Dey and Morrison, 1979).

$$\nabla \cdot \left[\frac{1}{\rho(x, y, z)} \nabla \varphi(x. y. z) \right] = $$
$$-I\delta(x - x_s)\delta(y - y_s)\delta(z - z_s) \quad (1)$$

where $\rho(x, y, z)$ is the resistivity distribution in 3D space, $\varphi(x. y. z)$ is the electrical potential, I is the point current source in the surface, and δ indicates the impulse function and the source location. To account for the 3D source characteristic, a spatial Fourier transform of the partial differential equations with respect to a range of wave numbers is performed along the strike direction:

$$\widetilde{\varphi}(x. k_y. z) = $$
$$\int_0^\infty \varphi(x. y. z) \cos(k_y y) \, dy \quad (2)$$

where $\widetilde{\varphi}$ indicates the transformed potential and k_y is the wave number with respect to y.
Applying the Fourier-cosine transformation to the 3D Poisson Equation (1) yields a 2D Helmholtz equation, given by:

$$\frac{\partial}{\partial x}\sigma(x. z) + \frac{\partial \widetilde{\varphi}}{\partial x} + k_y^2 \sigma(x. z)\widetilde{\varphi} - $$
$$\frac{\partial}{\partial z}\sigma(x. z)\frac{\partial \widetilde{\varphi}}{\partial z} = -\frac{I}{2}\delta(x - x_s)\delta(z - z_s) \quad (3)$$

The above equation is solved for a two-dimensional domain restricted by a mixed boundary condition. To numerically solve Equation (3), it is required to construct a discrete model in the form of a rectangular grid with nodes at the cell center. Then, the existing partial derivatives are replaced by finite-difference formulas. Having obtained discrete representations for the governing equations and boundary condition at all nodes, the transformed forward problem can be written as a system of equations (McGillivray and Oldenburg, 1990).

$$R\widetilde{\varphi} = q \quad (4)$$

R is a real sparse five-band symmetric matrix and q is the source vector. The recent equation has to be solved for the vector $\widetilde{\varphi}$ containing the potentials for all existing nodes. Since the matrix R is only dependent on the geometry and the physical property distribution, that is, for multiple current electrode positions this matrix remains unaltered, only one inverse of the matrix in terms of different wave numbers provides the solution to different sets of potential distribution for the different source positions. This action significantly reduces computational time. The solution $\widetilde{\varphi}$ is transformed from the wave number domain to the spatial domain following the procedure of Dey and Morrison (1979) and based on inverse cosine-Fourier transform,

$$\varphi(x. z) = $$
$$\frac{2}{\pi}\int_0^\infty \widetilde{\varphi}(x. k_y. z) \cos(k_y y) \, dK_y \quad (5)$$

with this approach, we are able to forward-model an electrical survey for any arbitrary conductivity distribution. In the following subsection, we discuss the inverse problem consisting in retrieving the subsurface conductivity distribution $\sigma(x. z)$ from observations $\varphi(x. z)$.

2-2. Inverse problem formulation

In this subsection, based on the forward modeling code proposed by Ghanati et al (2020), a flexible inversion strategy is developed. Let the observed data be represented by the vector $d \in \mathbb{R}^{m \times 1}$ contaminated by white Gaussian noise with zero-mean and variance ε^2, model parameters by the vector $m \epsilon \mathbb{R}^{n \times 1}$, and the non-linear forward operator by $f \in \mathbb{R}^{m \times n}$ mapping the model parameters to the noisy data. The ERT nonlinear inversion problem is inherently ill-posed resulting in non-unique estimates of the hydro-geophysical parameters. To numerically solve the inverse problem, we must consider data fidelity, model residual, and physical constraints to reduce instability of the inversion and the size/dimension of the model space to increase the chance of obtaining a geologically meaningful model. To that end, we form a weighted sum of the data fidelity Φ_d and the stabilizer function Φ_m using a weighting factor μ, and find the solution which

minimizes the objective function as given by:

$$\arg min_{\mathbf{m}\in\mathbb{R}^{n\times 1}} (\psi(\mathbf{m},\mu)) =$$

$$\arg min_{\mathbf{m}\in\mathbb{R}^{n\times 1}}\{\Phi_{\mathbf{m}} + \mu^{-1}\Phi_d\} \qquad (6)$$

equivalently

$$\arg min_{\mathbf{m}\in\mathbb{R}^{n\times 1}}(\psi(\mathbf{m},\mu)) =$$
$$\arg min_{\mathbf{m}\in\mathbb{R}^{n\times 1}}\left[(\mathbf{m} - \mathbf{m}_{apr})^T \mathcal{L}_m^T \mathcal{L}_m (\mathbf{m} - \mathbf{m}_{apr}) + \mu^{-1}\left\{(\boldsymbol{d} - f(\mathbf{m}))^T \Gamma^T \Gamma (\boldsymbol{d} - f(\mathbf{m}))\right\}\right] \qquad (7)$$

$\mathcal{L}_m$ is the constraint matrix defined as the first order roughening matrix to ensure a certain behavior of the model, $\Gamma \epsilon \mathbb{R}^{m\times m}$ is the data weighting matrix consisting of the inverse of the data error on the assumption that the noise for each experiment is independently but normally distributed, μ is the regularization parameter and $\mathbf{m}_{apr}$ allows the specification of a given reference vector of prior information for the model parameter $\mathbf{m}$. Because of the nonlinearity of the inverse problem, the inversion process starts with the linearization of the forward function $f(\mathbf{m})$ based on Taylor's series expiation. Given a trial model m^k, using Taylor's series expiation, we get:

$$f(\mathbf{m}^{k+1}) = f(\mathbf{m}^k) + \nabla f(\mathbf{m}^k)(\mathbf{m}^{k+1} - \mathbf{m}^k) \quad (8)$$

where $\nabla f(\mathbf{m}^k) = \frac{\partial f(\mathbf{m}^k)_i}{\partial \mathbf{m}_j^k}$ $(i = 1,2,\dots,m$ and $j = 1,2,\dots,n)$ is the Jacobian of $f(\mathbf{m})$ about the previous estimate $\mathbf{m}^k$ derived from truncating higher order of terms of Taylor's series expansion. The Jacobian matrix shows the variation of the forward response to the variation of model parameters. The construction of this matrix is very significant so that a part of the efficiency of the inversion process relies strongly on this Jacobian calculation routine.

Using Equation (7), the cost function is written as follows:

$$\psi(\delta\mathbf{m},\mu) = \arg min_{\delta\mathbf{m}\in\mathbb{R}^{n\times 1}}\{\mu^{-1}\|(\delta\boldsymbol{d} - J\delta\mathbf{m})\|_{\Gamma^{-1}}^2 + \|\mathcal{L}_m(\delta\mathbf{m})\|_2^2\} \qquad (9)$$

Where J denotes the Jacobian matrix, and $\delta d = [\log \boldsymbol{d} - \log f(\mathbf{m})]$.

Solving the objective function produces the following results (Aster et al, 2011).

$$\delta\mathbf{m}^{k+1} = \vartheta^k \times \{(J^T(\mathbf{m}^k)\Gamma^T\Gamma J(\mathbf{m}^k) + \mu\mathcal{L}_m^T\mathcal{L}_m)^{-1} \times J^T(\mathbf{m}^k)\Gamma^T\Gamma(\boldsymbol{d} - f(\mathbf{m}^k)) - \mu\mathcal{L}_m^T\mathcal{L}_m(\mathbf{m}^k - \mathbf{m}_{apr})\} \qquad (10)$$

where J^T is the transpose of matrix J, k shows the k-th iteration of the inversion process, $\delta\mathbf{m}^{k+1}$ is a search direction, and ϑ^k is the step length with positive value averting the iteration divergence. The Jacobian matrix or sensitvity function is computed using an efficient numerical approach based on the forward matrix calculation in the framework of the 2.5-D finite-difference electrical resistivity forward modeling. Appendix A provides a detail of constructing the sensitivity matrix corresponding to each datum point. Solving the inversion problem using the above relation may result in unrealistic estimates of resistivity distribution. More realistic solutions can be obtained by imposing physical constraints on model variations. Hence, it is necessary to use the transformation functions in the inversion algorithm in different iterations to avoid unrealistic model estimates. To this end, we follow the idea proposed by Kim and Kim (2011) to define the lower and upper bound constraints on the inverted model parameters. The process of minimization is implemented with a series of μ values aiming at choosing μ for which the smoothest model is achieved while the misfit Φ_d is kept at the desired level. The motivation for seeking the smoothest model is that one does not wish to be misled by features that appear in the model but are not essential in matching the noisy measurements. In other words, of all the possible solutions (i.e., solotions which adequately fit the observations within a certain tolerance), we seek the simplest model in the sense that it requires the least spurious features not required by the observed data. This strategy is often referred to as Occam's inversion wherein the inversion process is implemented in two steps: at the first step, the focus is on minimizing the misfit function to a prescribed tolerance (i.e., $\chi^2 = \|\mathbf{d} - f(\mathbf{m})\|_{\Gamma^{-1}}^2/m$, m is the size of the data vector, moves close to one) in terms of a range of the regularization parameters, and the second step continues minimization of the objective function while keeping the misfit function constant at the desired level. The proposed inversion algorithm is summarized in Table 1 in the context of a model-space Occam's method.

Table 1. Algorithm Pseudocode corresponding to the model-space Occam's inversion.

Inputs: Observed data $\boldsymbol{d}\epsilon\mathbb{R}^{m\times1}$,   model $\mathbf{m}_{apr}\epsilon\mathbb{R}^{n\times1}$ and data weighting matrix $\Gamma\epsilon\mathbb{R}^{m\times m}$
Outputs: Inverted model parameters $\mathbf{m}\epsilon\mathbb{R}^{n\times1}$ and resolution density matrix $\mathfrak{R}\epsilon\mathbb{R}^{n\times n}$
Initialization: define a range of μ_q ($q = 1, ..., N$), $\mathcal{L}_m$ (constraint matrix defined as the first order roughening matrix), $\mathbf{m}_{apr} = 0$ (when no *a priori* model or information is available) or $\mathbf{m}_{apr} = \mathbf{m}_{VES}$ ($\mathbf{m}_{VES}$ is the model derived from the inversion of vertical electrical sounding data), $\epsilon = 0.02$, $k = 1$, $\chi_0^2 = 0$
While $\chi^2 > 1$ or $\left(\left\|\chi_k^2 - \chi_{k-1}^2\right\|_2 / \left\|\chi_k^2\right\|_2\right) \leq \epsilon$ or maximum iteration is not reached **do**
Comput $\boldsymbol{d}^k = f(\boldsymbol{m}^{k-1})$
Compute $\delta\boldsymbol{d}$ the discrepancy between the measured apparent resisticity data and the calculated one
Compute the matrix $J(\boldsymbol{m}^{k-1})\epsilon\mathbb{R}^{m\times n}$ with respect to all model cells and meaurements
For μ_q, $q = 1, ..., N$ **do**
Compute the model perturbation $\delta\mathbf{m}$ using Equation (10)
Implement a linesearch algorithm to find the optimum value of ϑ
Update $\delta\mathbf{m} = \vartheta \times \delta\mathbf{m}$
Compute $\mathbf{m}^q = \mathbf{m}^{q-1} + \delta\mathbf{m}$
Compue the data fidelity term $\Phi_d = \|\mathbf{d} - f(\mathbf{m}^q)\|_{\Gamma^{-1}}^2$
End for
Choose the largest value for μ_q such $\chi^2 \leq 1$, otherwise select a μ_q minimizing Φ_d
$k = k + 1$
Set $\mathbf{m}^{k-1} = \mathbf{m}^q$
End while

3. Numrical experiments
In this section, we present a set of experiments using two simulated examples and a real case from the Shahid Abad area in Iran to demonstrate the performance and reliability of the inversion algorithm.

3-1. Synthetic data examples
Here, the observed data derived from the two synthetic models are generated using RESIP2DMODE, an open-source MATLAB code for 2.5-D forward modeling of resistivity and induced polarization data (Ghanati et al., 2020). The apparent electrical resistivity responses of the synthetic models are simulated using the linear dipole-dipole configuration from position 0 up to 100 m with fixed electrode spacings of 5 m up to 8 levels ($n = 1 - 8$, where n indicates the number of receiver-transmitter dipole separation) leading to a total of 132

measurements. For the 2.5-D forward modeling, we divide the model into a set of rectangular cells where the width of the work-area cells is the same as the unit electrode spacing and the depth of the cells logarithmically increases in the vertical direction. After the discretization, the model grid contains 22×99 regular cells. The first model (referred to as Example 1) consists of two rectangular bodies, one conductive (10 Ωm) and the other resistive (1000 Ωm), in a homogeneous medium of 100 Ωm as shown in Figure 1. The second example (referred to as Example 2) has more complex properties, which comprises a layered structure having an embedded low conductive layer and a buried high-conductive block in the middle of the section (see Figure 2(a)). Table 2 represents the geo-electrical parameters associated with Examples 1 and 2.

Table 2. Synthetic geo-electric parameters corresponding to Examples 1 and 2.

	Example 1			Example 2			
	Block 1	Block 2	Background	Layer 1	Layer 2	Layer 3	Block
Resistivity (Ωm)	10	500	100	320	2300	550	300

As a further concession to realistic field situations, the forward modeling responses are perturbed with 3 percent uncorrelated Gaussian-distributed noise of zero mean depending on the magnitude of each datum point. During the inversion process, lower and upper bounding constraints for the resistivity values are defined as $[\rho^{low} = 0, \rho^{upper} = 1000]$ Ωm and $[\rho^{low} = 0, \rho^{upper} = 3000]$ Ωm for the first and second examples, respectively. Figures 1(b) and 2(b) indicate the resistivity pseudo-sections of the noise-corrupted data corresponding to Examples 1 and 2, respectively. From the pseudo-sections, it is not possible to discern the true structures. To control the number of iterations during the inversion process, three stopping criteria are defined. That is, the inversion is terminated if 1) $\chi^2 \leq 1$ or 2) maximum iteration is reached or 3) $(\|\chi^2_k - \chi^2_{k-1}\|_2 / \|\chi^2_k\|_2) \leq \epsilon, \epsilon = 0.02$. The inversion begins with a uniform resistivity model ($\mathbf{m}_0$) derived from the geometric mean of the apparent resistivity data as the starting model. The sensitivity matrix is recalculated after each iteration, which is computationaly costly. Figures 1(c) and 2(c) show the resulting smooth inversion of the first and the second synthetic data, respectively.
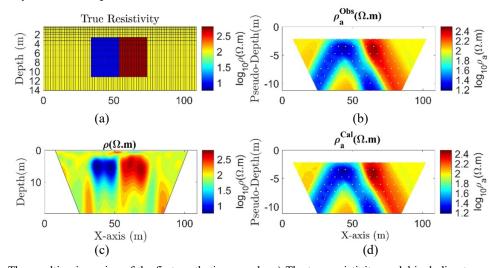

Figure 1. The resulting inversion of the first synthetic example; a) The true resistivity model including two rectangulare bodies, one conductive (10 Ωm) and the other resistive (1000 Ωm), in a homogeneous medium of 100 Ωm, b) The noise-contaminated synthetic data set in a pseudo-section form, c) The inverted model based on the model-space Occam's inversion, d) The theoretical data set in a pseudo-section form.
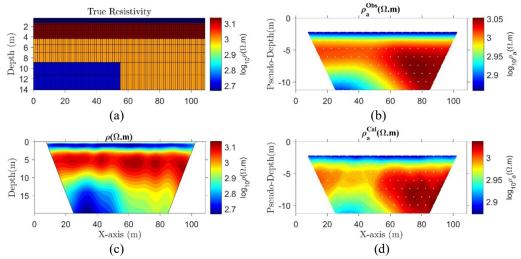

Figure 2. The resulting inversion of the second synthetic example; a) The true resistivity model including three horizontal layers with resistivity values ($\rho_1 = 320\,\Omega m, \rho_2 = 2300\Omega m, \rho_3 = 550\,\Omega m$) from the top-most to lowest layer and a conductive block of 300 Ωm, b) The noise-contaminated synthetic data set in a pseudo-section form, c) The inverted model based on the model-space Occam's inversion, d) The theoretical data set in a pseudo-section form.

From these figures, it is obvious that the main features and structures of both synthetic models are well reproduced and there are no undesirable features (artifacts) on the inverted resistivity tomograms. In the case of Example 1, the top surfaces of the two blocks are well resolved at a depth of about 2.8 m, which is highly consistent with the true model (2.67 m). Besides, the inversion algorithm correctly retrieves the boundaries of the horizontal layers and the buried conductive block corresponding to the second example. In both examples, the inversion algorithm requires 9 and 6 iterations to converge with the relative rms data misfit error $(RRMS = \sqrt{\frac{\sum_{i=1}^{m} \frac{(d-f(\mathbf{m}))_i^2}{d_i^2}}{m}})$ values of 1.4% and 4.5% associated with Examples 1 and 2, respectively. Furthermore, the resulting χ^2 score are $[\chi_1^2 = 1.1$ and $\chi_2^2 = 1.52]$, meaning that the inverted models adequately fit the observed data within the error bound (see Figure 3).

3-2. Field data example

In the previous section, we showed the functionality and accuracy of our inversion algorithm to synthetic data sets. Here, we provide a field example with known geology information aiming at demonstrating the capability and efficiency of the presented methodology in actual situations. The study area is located in the rural district of Shahid Abad in Qazvin province, Northwest Iran. At this site, based on the drill holes, the geology of the area comprises an unsaturated zone with a thickness of 1.5 m, followed by a fresh-water bearing layer consisting of fine sand and clayey sand until a depth of 5 m, underlined by a 4.5 m mudstone followed by mudstone mixed with siltstone layer until the bottom of the borehole. The acquisition of the 2D electrical resistivity data was conducted with the DMT RESECS resistivity instrument and 48 stainless steel electrodes. We used the Wenner array for its very good signal-to-noise ratio with an electrode spacing of 2 m and interval separation of 2 m up to 30 m. A total of 364 measurements were taken. To construct the data weighting matrix using the measurement errors, in addition to normal measurements, a total of 364 reverse readings were also collected. It should be noted that in the Wenner array due to the different geometry of transmitter and receiver electrodes in normal and reverse measurements, it would be expected that the noise in the reverse measurements is larger than the noise in the forward measurements. Hence, regarding the Wenner array, care must be taken when using the procedure of reciprocity. To reduce the influence of noise on the inversion result, the resistivity measurements were filtered to remove noisy data. Filtering criteria were set to discard data whose injected current was less than 10 mA or whose standard deviation derived from the stacking errors was larger than 5%. Note that stacking errors are given by the averaging of stacks obtained by the electrical resistivity collection instrument. We follow the inversion strategy described for synthetic experiments.

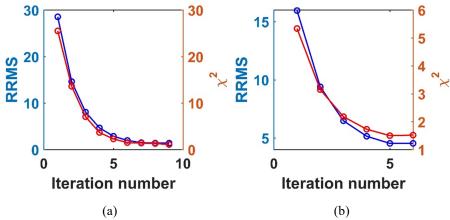

(a)   (b)

Figure 3. The resulting relative rms misfit error (blue) and χ^2 score (red) versus iteration number corresponding to a) Example 1 and b) Example 2.

The linearized inversion begins with a half-space resistivity of 100 Ωm, being the geometric average value of the measured electrical resistivity data. The grid discretization used for the inversion corresponds to 2000 model parameters on a rectilinear mesh. In Figures 4 (a) and (b) the observed resistivity data and the inverted resistivity tomogram obtained from the model-space Occam inversion algorithm are shown. We can see an approximately 2-m-thick layer with high resistivity values, which is assigned to the vadose zone (unsaturated layer). Furthermore, there is a 5-m-thick layer characterized by low resistivity values in the middle of the section. This layer is consistent with the presence of a water-saturated clayey sand layer existing at the site. It is also observed that the aquitard layer appears with higher resistivity values than the aquifer layer, which is due to the existance of the mudstone layer. Comparing the inversion results with a nearby lithology borehole information, a satisfactory match can be seen between the inverted resistivity tomogram and the ground truth.To see also the role of *a* priori information, the inversion scenario is implemented by incorporating a priori

information based on a geo-electrical sounding data set conducted in the vicinity of the 2D resistivity profile. From the resulting inversion of the geo-electrical sounding data (see Ghanati and Müller-Petke, 2021), we use a four-layer reference model with the geo-electrical parameters ($\rho_1 = 55$ Ωm, $h_1 = 1.3$ m; $\rho_2 = 12$ Ωm, $h_2 = 5.2$ m; $\rho_3 = 40$ Ωm, $h_3 = 4.8$ m; $\rho_4 = 21$ Ωm). The final inverted resistivity section incorporating the reference model is illustrated in Figure 5(b). By incorporating the reference model, Figure 5 indicates that we better resolve the lower and upper boundary of the aquifer. It is worth mentioning that in the resistivity section, the decrease of resolution with increasing depth may give rise to erroneous layer boundaries reconstruction. Figure 6(a) shows that the inversion process before including the reference model converged within five iterations reducing the χ^2 score from 10.2 (RRMS = 9.37%) to 1. 3 (RRMS = 5.3%), while with incorporating the *a priori information* the convergence of the inversion algorithm is realized with six iterations reducing the χ^2 score from 10 (RRMS = 15.1%) to 3.1 (RRMS = 9.2%) (see Figure 6(b)).
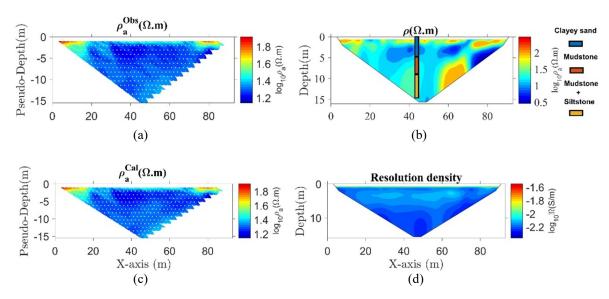

Figure 4. Inversion results of the field data without incorporating the reference model; a) The field data in a pseudo-section form, b) Inverted tomogram of the field data, c) The theoretical data set in a pseudo-section form, d) Resolution density $\Re$ distribution corresponding to the inverted model. The water table measured in the borehole can be found in depth of about 3 m from the subsurface.
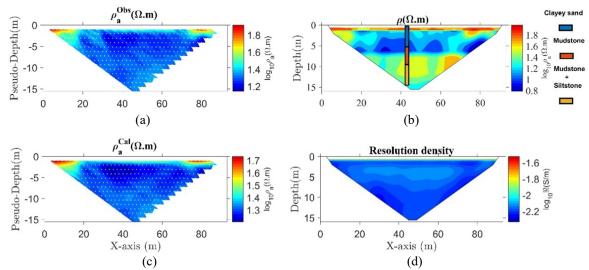
Figure 5. Inversion results of the field data with incorporating the reference model; a) The field data in a pseudo-section form, b) Inverted tomogram of the field data without incorporating the reference model, c) The theoretical data set in a pseudo-section form, d) Resolution density $\Re$ distribution corresponding to the inverted model. The water table measured in the borehole can be found in depth of about 1.5 m from the subsurface.
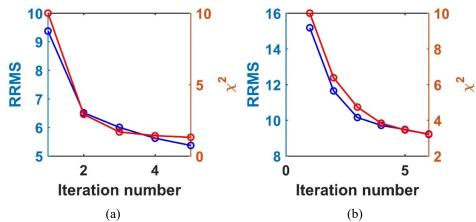

Figure 6. The resulting relative rms misfit error (blue) and χ^2 score (red) versus iteration number obtained from the inversion of the field data (a) before and (b) after incorporating the reference model.

Furthermore, to mathematically evaluate the resulting models, we follow the idea proposed by Zhdanov & Tolstaya (2006) and applied to the multi-expotensial inversion of surface-NMR data (Fallahsafari et al., 2020). This algorithm provides a posteriori appraisal of the quality of the inverted models by calculating a distribution of the resolution density as:

$$\Re = [\sum_{j=1}^{m}|\Lambda_{\mu ij}|^2]^{-\frac{1}{2}}/\|\boldsymbol{d}\| \qquad (11)$$

where $\Re$ stands for the resolution density distribution with the unit of $\frac{1}{[\Omega m]}$ or $[S/m]$, $\boldsymbol{\Lambda}_\mu$ is the generalized inverse of the Jacobian matrix so that $\boldsymbol{\Lambda}_\mu = (\boldsymbol{J}^T(\mathbf{m})\Gamma^{\mathrm{T}}\Gamma\boldsymbol{J}(\mathbf{m}) + \mu\mathcal{L}_m^T\mathcal{L}_m)^{-1} \times \boldsymbol{J}^T(\mathbf{m})\Gamma^{\mathrm{T}}\Gamma$. By knowing the

distribution of the resolution density in the area of the inversion, it is possible to identify the parts of the inverse model that are well resolved (and therefore physically interpretable) and the parts that are poorly resolved.

Using the general resolution theory outlined above, Figures 4(d) and 5(d) illustrate the depth and lateral variations of the resolution density $\Re$ corresponding to the area of the inversion shown in Figures 4(b) and 5(b), respectively. One can see that the resolution density decreases at the bottom and the sides of the inverted resistivity tomogram.

4. Conclusions
In this study, we have provided a smoothness-constrained inversion algorithm

referred to as Occam's method aiming at 2.5-D electrical resistivity inversion. We demonstrated that by searching the solution of the smoothest model, one does not wish to be misguided by structures that appear in the inverted model but are not essential in matching the noise corrupted observations. To verify the efficiency and accuracy of our developed ERT inversion code package (including the forward modeling algorithm, the Fréchet derivative computation, and the inversion algorithm), we applied the algorithm to a set of synthetic data examples and a real field data set. The numerical results demonstrated that the presented inversion algorithm provides stable inversion results and an acceptable representation of the main features and structure of the models without producing spurious effects. In the case of real data inversion, we followed two scenarios: 1) data inversion without any *a priori* information (i.e., $\mathbf{m}_{apr} = 0$), and 2) data inversion with incorporating a reference model constructed based on the geological information and geo-electrical sounding data in the vicinity of the 2D resistivity profile. It was demonstrated that the inclusion of the reference model gives rise to better retrieval of the lower and upper boundaries of the saturated media (aquifer). Furthermore, to deal with the reliability of the inverted resistivity tomogram, a model sensitivity analysis was implemented based on the resolution density distribution. In summary, regardless of the theoretical aspects presented in this paper, the main contribution of this work is the better resolving of subsurface structures in terms of the resistivity distribution through a smoothness-constrained inversion strategy without the presence of unnecessary features (artifacts) in the inverted models.

References

Aster, R. C., Borchers, B. and Thurber, C. H., 2011, Parameter estimation and inverse problems: 2nd Edition, Elsevier Academic Press.

Chambers, J.E., Kuras, O., Meldrum, P.I., Ogilvy, R.D. and Hollands, J., 2006, Electrical resistivity tomography applied to geologic, hydro-geologic, and engineering investigations at a waste-disposal site. Geophysics, 71(6).

Constable, S.C., Parker R.L. and Constable, C.G., 1987, Occam's inversion: A practical algorithm for generating smooth models from electromagnetic sounding data. Geophysics, 52, 289-300.

Dahlin, T. and Zhou, B., 2001, A numerical comparison of 2D resistivity imaging with eight electrode arrays. In 7th Meeting of the Environmental and Engineering Geophysical Society (European Section), pages 977–983.

deGroot Hedlin, C. and Constable, S., 1990, Occam's inversion to generate smooth, two-dimensional models from magnetotelluric data. Geophysics, 55(12), 1613–1624.

Dey, A. and Morrison, H.F., 1979, Resistivity modelling for arbitrarily shaped two-dimensional structures. Geophysical prospecting, 27(1), 106-136.

Fallahsafari, M., Ghanati, R., Hafizi, M.K. and Müller-Petke, M., 2020, A fast multi-exponential inversion of magnetic resonance sounding using iterative Lanczos bidiagonalization algorithm. Journal of Applied Geophysics, 175.

Ghanati, R., Azadi, Y. and Fakhimi, R., 2020, RESIP2DMODE: A MATLAB-Based 2D Resistivity and Induced Polarization Forward Modeling Software, Iranian Journal of Geophysics 13 (4), 60-78.

Ghanati, R. and Müller-Petke, M., 2021, A Homotopy continuation inversion of geo-electrical sounding data, Journal of Applied Geophysics, 191. https://doi.org/10.1016/j.jappgeo.2021.10 4356.

Günther, T., Rücker, C. and Spitzer, K., 2006, Three-dimensional modelling and inversion of DC resistivity data incorporating topography - II. Inversion. Geophysical Journal International, 166(2), 506–517.

Kim, H.J. and Kim, Y.H., 2011, A unified transformation function for lower and upper-bounding constraints on model parameters in electrical and electromagnetic inversion: Journal of Geophysics and Engineering. 8, 2126.

Loke, M.H. and Barker, R.D., 1996, Rapid least-squares inversion of apparent resistivity pseudo-sections by a quasi-Newton method. Geophysical

Prospecting, 44, 131–152.

McGillivray, P.R. and Oldenburg, D.W., 1990, Methods for calculating Fréchet derivatives and sensitivities for the non-linear inverse problem: a comparative study. Geophys. Prospect., 38(5):499–524.

Oldenborger, G.A., Routh, P.S. and Knoll, M.D., 2007, Model reliability for 3D electrical resistivity tomography: application of the volume of investigation index to a time-laps monitoring experiment. Geophysics, 72 (4), F167–F175.

Pang, Y., Nie, L., Liu, B., Liu, Z. and Wang, N., 2020, Multiscale resistivity inversion based on convolutional wavelet transform, Geophysical Journal International, 22(1), 132–143.

Pelton, W. H., Rijo, L. and Swift, C. M., 1978, Inversion of two-dimensional resistivity and induced-polarization data. Geophysics, 43(4), 788–803.

Scales, J.A. and Snieder, R., 1997, To Bayes or not to Bayes? Geophysics 63, 1045–1046.

Smith, N.C. and Vozoff, K., 1984, Two dimensional DC resistivity inversion for dipole-dipole data IEEE Trans.

Gemeience Remote Sensing, 22 21-8.

Tong, L.T. and Chieh-Hou, Y., 1990, Incorporation of topography into two-dimensional resistivity inversion, Geophysics, 55, 354-361.

Tripp, A.C., Hohmann, G.W. and Swift, C. M., 1984, Two dimensional resistivity inversion. Geophysics, 49, 708-1717.

Wilkinson, P.B., Chambers, J.E., Lelliott, M., Wealthall, G.P. and Ogilvy, R.D., 2008, Extreme sensitivity of cross-hole electrical resistivity tomography measurements to geometric errors. Geophysical Journal International, 173 (1), 49–62.

Zhdanov, M. and Tolstaya, E., 2006, A novel approach to the model appraisal and resolution analysis of regularized geophysical inversion. Geophysics 71, 79–90.

Zhou, B. and Dahlin, T., 2003, Properties and effects of measurement errors on 2D resistivity imaging surveying. Near Surface Geophysics, 1 (3), 105–117

Zhou, J., Revil, A., Karaoulis, M., Hale, D., Doetsch, J. and Cuttler, S., 2014, Image-guided inversion of electrical resistivity data, Geophysical Journal International, 197, 292–309.

Appendix (A)

In this appendix, we provide a brief description of the construction of the sensitivity function. Recall the final system of equations derived from the assembly of the element equations, which has the general form (Equation 4):

$$\boldsymbol{R} \cdot \widetilde{\varphi}(x, k_y, z) = \boldsymbol{q} \tag{A-1}$$

Where $\boldsymbol{R}$ is the capacitance matrix, $\widetilde{\varphi}$ is the Fourier-transformed vector potential for a given wave number (k_y) and $\boldsymbol{q}$ is the source term with a non-zero element corresponding to the source electrode position. Partial differentiation of the finite-difference equation with respect to the conductivity σ_n of a parameter n yields:

$$\frac{\partial}{\partial \sigma_n}(\boldsymbol{R} \cdot \widetilde{\varphi}(x, k_y, z)) = \frac{\partial \boldsymbol{q}}{\partial \sigma_n} \tag{A-2}$$

and application of the chain rule (the source term is independent of the conductivity of the parameters) yields:

$$\boldsymbol{R}' \cdot \widetilde{\varphi}(x, k_y, z) + \boldsymbol{R}\widetilde{\varphi}'(x, k_y, z) = 0 \tag{A-3}$$

Whereas the capacitance matrix $\boldsymbol{R}$ and the Fourier-transformed vector potential $\widetilde{\varphi}(x, k_y, z)$ are already known from the solution of the forward problem, the derivative of the measured potential with respect to each model cell can be easily and efficiently calculated. Furthermore, based on the structure of the capacitance matrix $\boldsymbol{R}$, the matrix $\frac{\partial \boldsymbol{R}}{\partial \sigma_n}$ with twelve non-zero elements has the size of $n_z \times n_x \times n_z \times n_x$, where n_z and n_x are the number of model cells in the z and x directions, respectively.